

Basis Function Based Data Driven Learning for the Inverse Problem of Electrocardiography

Tommy Peng, Avinash Malik, Laura Bear, and Mark L. Trew

Abstract—Objective: This paper proposes an neural network approach for predicting heart surface potentials (HSPs) from body surface potentials (BSPs), which re-frames the traditional inverse problem of electrocardiography into a regression problem through the use of Gaussian 3D (G3D) basis function decomposition. **Methods:** HSPs were generated using G3D basis functions and passed through a boundary element forward model to obtain corresponding BSPs. The generated BSPs (input) and HSPs (output) were used to train a neural network, which was then used to predict a variety of synthesized and decomposed real-world HSPs. **Results:** Fitted G3D basis function parameters can accurately reconstruct the real-world left ventricular paced recording with percent root mean squared error (RMSE) of $1.34 \pm 1.30\%$. The basis data trained neural network was able to predict G3D basis function synthesized data with RMSE of $8.46 \pm 1.55\%$, and G3D representation of real-world data with RMSE of $18.5 \pm 5.25\%$. Activation map produced from the predicted time series had a RMSE of 17.0% and mean absolute difference of 10.3 ± 10.8 ms when compared to that produced from the actual left ventricular paced recording. **Conclusion:** A Gaussian basis function based data driven model for re-framing the inverse problem of electrocardiography as a regression problem is successful and produces promising time series and activation map predictions of real-world recordings even when only trained using Guassian data. **Significance:** The HSPs predicted by the neural network can be used to create activation maps to identify cardiac dysfunctions during clinical assessment.

Index Terms—Electrocardiogram decomposition, Pro-arrhythmic risk, Gaussian Mesa Functions, Electrocardiogram prediction.

I. INTRODUCTION

Predicting heart surface potentials (HSPs) from body surface potentials (BSPs) is termed as the inverse problem of electrocardiography [1]. Achieving good predictions would allow for non-invasive cardiac surface assessments which can assist in source localization for cardiac procedures such as ablation [2]. The forward relationship between HSP and BSP is described in Eq 1, where A characterizes the geometric relationship between the body and heart surface potential at any instance in time. The problem of estimating A^{-1} given instances of concurrent BSPs and HSPs is known to be ill-posed and

Tommy Peng is with the Department of Electrical and Computer Engineering, University of Auckland. E-mail: tpen280@aucklanduni.ac.nz.

Avinash Malik is with the Department of Electrical and Computer Engineering, University of Auckland.

Laura Bear is with IHU-LIRYC.

Mark L. Trew is with the Auckland Bioengineering Institute, University of Auckland.

Manuscript submitted November 10, 2020. This work was funded by the National Science Challenges, Science for Technological Innovation, NZ, grant 3713917. Mark L. Trew was supported by a grant from the Fondation Leducq.

therefore difficult to solve [1], [3]. Current approaches such as electrocardiographic imaging (ECGI) [4], [5] estimates the HSP (\hat{HSP}_λ) by minimizing the error or L2-norm residual with an additional a penalty term λR as shown in Eq 2, where λ is the regularization parameter and R is the regularizer. Regularization parameters must be chosen carefully, as too large of a regularization parameter results in overly smooth HSP predictions, and too small of a regularization parameter results in oscillating HSP predictions [1], [6]. ECGI resolves this issue by using a number of electrophysiological constraints and special smoothing operators [5]. While methods exist for estimation of the quasi-optimal regularization parameter, there is no single estimation technique which performs best for all geometries and signal-to-noise ratios (SNRs) [7], [8], [3].

$$BSP = A \times HSP \quad (1)$$

$$\hat{HSP}_\lambda = \|BSP - A \times HSP\|_2^2 + \lambda R \quad (2)$$

Ultimately, predicting HSPs from BSPs can be framed as a regression problem [9], where we find some approximation for A^{-1} given simultaneously observed BSP-HSP pairs. Here, we *hypothesize* that the prediction of HSPs from BSPs (traditionally, the inverse problem) can be framed as a forward problem and solved by using a data driven model. Neural networks have been shown to be effective at solving data driven regression problems [10]. During training, neural networks implicitly learn the linear or non-linear relationship between HSP and BSP. This data driven approach for solving the inverse problem of electrocardiography is successful in recovering HSPs from BSPs [6], [11], [19].

However, a common **problem** encountered by the neural network approach is the richness of heart states found in the training data set [11], [2], [12]. Neural networks can only predict data similar to that found in the training set, therefore training a neural network to solve the cardiac inverse problem require a large amount of BSP and HSP recordings across different heart states. Unfortunately, detailed simultaneous HSP and BSP recordings from real hearts in different heart states are limited. As a solution, we propose to decompose the HSPs into a basis function across heart conditions and train the neural network with examples from that common space. Decomposition is important because while a particular heart state HSP may not be in the training set, the decomposed HSP basis function will likely have been. To that end, Gaussian basis functions have been shown to be effective at capturing cardiac signals [13], [14]. These basis functions can be used to model and generate real-world-like cardiac signals under different drug and disease states [15], [16]. Furthermore,

boundary element forward models using recording electrode geometries have been relatively successful in capturing the HSP to BSP relationship (Laura/Mark's forward model). This relationship allows us to generate training data pairs for the neural network.

We aim to generalize this solution for heart surface potentials using signal decomposition, signal projection, and neural networks. **Our contributions** are: 1. we show that HSPs can be effectively modelled and generated using Gaussian 3D basis functions; 2. we demonstrate that a single neural network trained on Gaussian basis functions can be used to predict never seen before physiologically relevant synthesized HSPs from BSPs; 3. we extend the prediction of HSPs from signals recorded in the real-world. We show that a data drive model trained using a suitable basis function (HSPs) and forward model (BSPs) can be effective for prediction of real-world HSPs from BSPs. In essence, our approach is predicting the output of a system, by learning the system characteristics through basis function driven responses.

II. METHODS

Figure 1 is a visual representation of the Gaussian basis neural network pipeline. Note here that the forward model is only being used for data generation purposes. The training and testing data can ultimately be replaced by recordings from real world experimental recordings.

A. Data Context

The original heart-in-tank data was recorded by Bear et. al. at IHU-LIRYC [17]. In the experiment, an excised pig heart was perfused in Langendorff mode, with an epicardial electrode sock of 108 electrodes attached to the ventricles. The heart was placed inside a human-shaped torso tank with 128 body surface electrodes. Simultaneous body and heart signals were recorded. The geometry of the epicardium and body surface was extracted from CT full form images.

Heart and body surfaces are abstracted to regular 2D matrix of points. These provide a standard context for training and applying neural network data models. They are also consistent with the topology of electrode matrices used for electrical mapping on both the heart and body surfaces [17]. Consequently, the heart surface is represented by a grid of 9-by-12 points and the body surface a grid of 16-by-16 points. The body surface grid is arbitrary and has more points than typical numbers of body surface electrodes. See Supplementary Materials for more details on the 2D abstractions.

B. Neural Network Data Model

1) *Neural Network Design and Implementation:* A neural network with a dense fully connected one hidden layer architecture was implemented in Python using Keras with a Tensorflow back-end. This architecture is mathematically proven to be capable of approximating any smooth continuous function given enough neurons and appropriate activation functions [18], [19]. The network is designed to capture the relationship in the x - y plane between 2D Gaussian basis

HSP and its simultaneous 2D BSP. Therefore, the input layer consists of 256 neurons corresponding to the 16-by-16 body surface 2D abstraction points, and the output layer consists of 108 neurons corresponding to the 9-by-12 heart surface electrodes. Neuron bias was turned off, as we expect a zero BSP input to produce a zero HSP output.

2) *Training Data Generation:* The Gaussian basis function [13], [15] and Gaussian mesa functions [14] have been used in the past to successfully decompose cardiac signals. The decomposition process allows for cardiac signals from different cardiac states to be expressed in a common parameter space, which allows for objective representation and quantitative comparison of signals. Here, we consider a Gaussian 3D basis function (G3D) for describing 3D cardiac signal matrices as it is smooth and continuous in both space and time. We define the G3D to be Eq 3, where x and y are the 2D abstraction dimensions, t is the normalized heartbeat time in the recording. Normalized heartbeat time at a sample can be calculated by dividing the current sample number by the total number of samples in the recording of the heartbeat, and can vary between 0 and 1 for a heart beat. Parameter \mathcal{A} is the amplitude, μ_i is the location of the Gaussian peak in the i dimension ($i \in x, y, t$), σ_i is the standard deviation or width of the Gaussian in the i dimension ($i \in x, y, t$) expressed relative to the size of that dimension. Here, we limit σ_x to be equal to σ_y to reduce the number of impulses needed to train the neural net.

$$G3D(x, y, t) = \mathcal{A} \times \exp\left(-\left(\frac{(x - \mu_x)^2}{2\sigma_x^2} + \frac{(y - \mu_y)^2}{2\sigma_y^2} + \frac{(t - \mu_t)^2}{2\sigma_t^2}\right)\right) \quad (3)$$

HSP training data was synthesized from G3D basis function parameters. The G3D training data included components with peaks (μ) at each combination of integer value of the x (i.e. 1-9) and integer value of the y (i.e. 1-12) dimension. The σ_x and σ_y at each peak location was allowed to vary in 0.02 intervals between 0.01 and 0.5. μ_t was set to 0.5 and σ_t was set to 0.3 for all basis components, this was done so that the training data would always have a non-zero x - y plane 2D surface with the peak located at the temporal center. Amplitude (\mathcal{A}) was allowed to be 1 or -1, due to the real-world HSPs exhibiting both positive and negative potentials for a single heartbeat recording. The training data generation used all combinations of given μ , σ , and \mathcal{A} values. This generated a total of 129600 x - y plane 2D HSPs.

The calculation of heart surface potentials given body surface potentials uses a volume conductor torso model [20]. The model is based on a heart in a torso tank experimental set up [17]. The specific model is not a critical component of this work and could be replaced by other models or experimental heart and body surface recordings. The 129600 HSPs samples were passed through the volume conductor forward model to produce 129600 BSP-HSP pairs in the training set, each containing a Gaussian basis HSP and its simultaneous BSP.

3) *Training Regime:* A 70-30 training-validation split was applied to the training data. A 0.1 dropout rate was im-

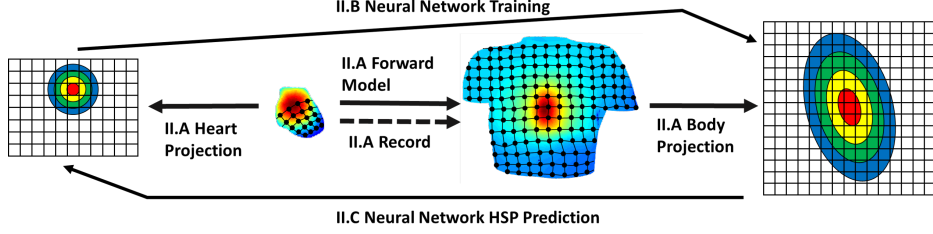


Fig. 1: Summary neural network pipeline.

plemented to reduce over-fitting. The hyperparameters for the neural net were tuned through grid search of possible hyperparameter pairings. The grid search was performed in Python with *GridSearchCV* from scikit-learn. The hyperparameter search space can be found in Table I, with best hyperparameters highlighted in green. Training was done using the Adaptive Momentum Estimation (ADAM) optimizer with root mean squared loss function. Training was completed over 100 epochs.

TABLE I: Hyperparameter Search Space

Hidden Neurons	[100, 150, 200, 250, 300, 350, 400]
Activation Function	[ReLU, Sigmoid, TanH]
Regularization	[None, L1, L2]
Batch Size	[16, 32, 64]
Learning Rate	[0.1, 0.01, 0.001]

C. Predictions using Parameterized Neural Networks

Prediction was done using the testing data sets, which were **not** presented to the neural network during training. During prediction, the input to the neural network is the 2D BSP surface, and the output from the neural network is the 2D HSP surface. All predicted HSPs were evaluated using error, which was calculated per 2D potential surface (x - y plane) by using percent root mean squared error (RMSE) found in EQ 4, where \hat{p} is the predicted or model generated 2D signal surface and p is the ground truth.

$$RMSE(\hat{p}, p) = 100 \frac{\sqrt{mean((\hat{p} - p)^2)}}{max(p) - min(p)} \quad (4)$$

1) *Pure Moving Gaussians*: In order to create a testing set with physiologically relevant generated Gaussian based time series, we synthesized 3D matrices of 9-by-12-by-100 size in which the peak of the Gaussian in the x , y dimensions moves in a straight line between two points (p1 to p2) on the heart electrode grid. The combination of points can be found in Table II, and 2D contour representation of the Gaussian basis function at different points along the 100 samples in the t dimension for path 1 can be seen in Fig 2. The σ_x and σ_y was set to 0.1768 for the synthetic HSPs for this moving Gaussian test data set. The paths were designed to reflect different pacing locations commonly found in clinical settings such as sinus, right ventricle, and left ventricle. The synthesized HSPs in the testing set were passed through the volume conductor forward model for their respective BSPs. This resulted in 600 x - y plane 2D surface BSP-HSP pairs in the pure Gaussian testing set. These 2D surface BSPs were

used as the input for the neural network to predict 2D surface HSPs.

TABLE II: x , y Dimension Location of Test I Points

Path	1	2	3	4	5	6
p1	[1, 1]	[1, 6]	[1, 12]	[4.5, 1]	[4.5, 12]	[9, 1]
p2	[9, 12]	[9, 1]	[1, 6]	[9, 12]	[9, 1]	[9, 12]

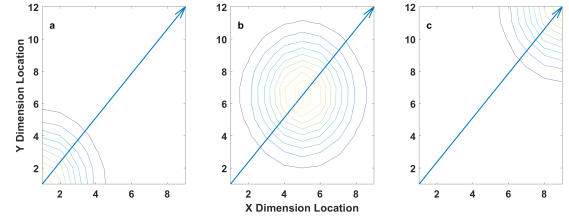


Fig. 2: Synthesized moving Gaussian data path 1 (from point [1, 1] to [9, 12]) with contours of the moving Gaussian. a) first sample of the moving path with peak centered at point 1, 1; b) 50 samples into the moving path with peak centered at point 5, 6.5; c) last sample of the moving path with peak at 12, 12.

Here, we explore the effects of modifying the testing and training data on the predicted HSPs in the following ways:

- 1) **Noise Robustness Test**: This is a modification on the test data. Signals recorded in the real world are often noisy, and that noise often contributes to poor predictions from neural networks. Similar to [12], forward model BSPs from the set of moving pure Gaussian signals were augmented with Gaussian white noise with MATLAB's *awgn* at 2dB, 5dB, 10dB, 20dB, and 50dB signal-to-noise-ratio (SNR), to create an additional robustness test dataset to observe neural net sensitivity arising from errors in BSP measurement.
- 2) **Geometry Robustness Test**: This is a modification on the test data. Often times during real-world experiments, there is noise in the geometry measurements of the heart and body. We simulate changes or measurement errors in heart body geometry through: 1. shifting the heart location within the forward model towards the back of the body at 5mm increments between 0 and 40mm; 2. rotating the heart within the forward model at 10° increments between -40° and 40°. The rotation axis was found using principle component analysis on the heart electrode locations in MATLAB. A positive rotation is clockwise along the axis, while a negative rotation is counterclockwise along the axis. The subsequent altered forward models were then used to produce BSPs from

HSPs along all 6 paths of the moving Gaussian testing set.

3) **Reduced Training Set Test:** Here, explore how reducing the training set would effect the prediction results. It is well known that an effective training data set for neural networks includes examples from all expected prediction outcomes [21]. We perform 3 reduction schemes for the x - y dimension peak location as shown in subplots b, c, d of Fig 3. We split the original G3D training set into 25 different σ reduction schemes consisting of training sets with a single x - y dimension σ at 0.02 intervals between 0.01 and 0.5 for HSPs. Each of the reduced training sets were used to train a separate neural network.

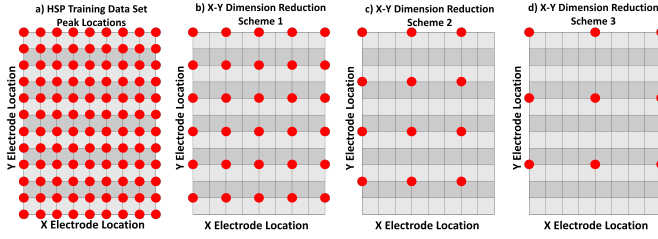


Fig. 3: The locations of training set G3D peak (μ) locations in the x - y (9-by-12) plane of the HSP surface. Red dots indicate the points in the x - y plane with a training set G3D peak. a) original training set from Section II-B1; b) reduction scheme 1; c) reduction scheme 2; d) reduction scheme 3.

The prediction results from the three data modification tests were compared against the pure moving Gaussian predictions from the neural net trained on the full training set. The results from the geometry robustness and reduced training set tests were evaluated by comparing the difference in signal peak locations in the 2D x - y plane.

2) *Experimental Recorded Data:* In this study, we make use of the left ventricular (LV) paced averaged beat recording from the experimental data [17] which is 649 samples in length recorded at a sampling rate of 2048Hz. This resulted in an LV HSP recording matrix of 9-by-12-by-649 after 2D abstraction at each sample in time. The 9-by-12-by-649 LV HSP matrix was fitted to G3D basis functions through an extension of the generalized orthogonal forward regression (GOFR) technique [14], [16]. The potential values were normalized between -1 and 1 while maintaining scale. To fit each G3D component, the current unexplained signal was first correlated against a library of G3D basis functions. A description of the library can be found in the Supplementary Materials. Then, the library function with the largest absolute correlation value was set as the initial point for loss function minimization using MATLAB's *fmincon*. Sum of squared differences (Eq 5), where v is the 1D form of the 3D matrix to be fitted and \hat{v} is the 1D form of the current fit of the 3D matrix, was used as the loss function. The bounds of optimization are shown in Table III.

TABLE III: Table of *fmincon* Optimization Bounds

Bound	μ_x	μ_y	μ_t	\mathcal{A}	σ_{xy}	σ_t
Upper	9	12	1	Max pot.	0.5	0.5
Lower	1	1	0	Min pot.	0	0

The bounds on μ limits the peak of the G3D components to always be contained within the recording, the \mathcal{A} bounds allow the amplitude of the G3D peak to vary between the range of potentials within the recording, and the σ bounds allow fitted G3D components to have visible effect throughout the whole recording. The bounds chosen here are similar to those found in [16], which have been shown to be effective for describing electrocardiographic signals. The fitted G3D component was then subtracted from all basis functions in the G3D library and the unexplained signal. The process iterated until the number of predefined G3D components were fit to the 3D recording matrix. The final G3D fit of the recording was evaluated per 2D potential surface (x - y plane) using percentage root mean squared error (*RMSE*) where the range ($\max(p) - \min(p)$) is 2 due to the normalization of potential between -1 and 1.

$$SSD(v, \hat{v}) = \sum (v - \hat{v})^2 \quad (5)$$

The left ventricular averaged heartbeat recording HSP was fitted with 100 G3D components. The 649 time instances of x - y plane 2D HSP surface for each of the 100 G3D component were individually passed through the volume conductor forward model to simulate their respective BSPs. This testing set created a testing set of 64900 x - y plane 2D surface BSP-HSP pairs. These 2D surface BSPs were used as the input for the neural network to predict 2D surface HSPs. Predicted real-world HSPs were evaluated via activation time, which is defined to be the time point for the most negative gradient (dV/dt).

III. RESULTS

A. Prediction of Moving Pure Gaussian HSPs

This section shows the prediction results for the moving pure Gaussian testing set. Fig 4 show the root mean squared error (RMSE) between the predicted and generated pure moving Gaussian HSPs. Across the 6 paths from Table II, the mean RMSE is $8.46 \pm 1.55\%$. An example of time series comparison for path 3 can be seen in Fig 5.

B. Robustness Tests

For the noise robustness test, the moving Gaussian signal augmented with white noise (Section II-C1) is supplied as the input to the basis function data trained neural network, with the generated moving pure Gaussian HSP set as the expected prediction outcome. The RMSE across all 6 paths at different noise levels can be found in subplot a of Fig 6. As expected, the error associated with the prediction decreases as the noise level decreases. Subplot b from Fig 6 shows an example of the HSP time series predicted based on BSPs with varying noise levels.

For the geometry robustness test, the prediction is carried out using the neural network trained with the training set with BSP-HSP pairs found with the forward model with no shift or rotation; however, the testing set is produced with forward models with rotations or shifts in the heart location as described in Section II-C1. Subplot a of both Fig 7 and Fig 8 show that the error of prediction increases as the

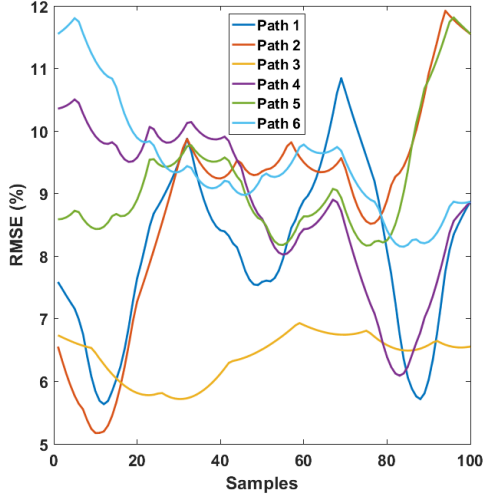


Fig. 4: RMSE for the predicted 2D sample slices (along x-y axis) for the G3D synthesized HSPs moving from point to point. The path numbers correspond to those found in Table II.

change in heart geometry increases. Subplot b of Fig 7 shows that the predicted time series share similar morphology, but are increasingly different in amplitude for as shifts increase between 0mm and 40mm. Subplot b of Fig 8 shows that a negative rotation angle increases the amplitude and decreases the Gaussian width of the signal in the time domain, while a positive rotation angle decreases the amplitude and increases the Gaussian width of the signal in the time domain.

C. Effects of Reduced Training Sets

For peak location reduction schemes, as an intuitive guide, Fig 9 shows a subsection of the electrode grid formed by four neighbouring electrodes (shown as red circles). The training set includes examples of G3D basis functions with peaks at the electrodes. The application of the peak location reduction schemes shown in Fig 3 can then be thought of as increasing the distance between neighbouring electrodes (d_x and d_y). In Fig 9, if we want to predict a HSP Gaussian with peak that is not at any of the electrodes (shown as the yellow star), the maximum Euclidean distance error in peak location that can be made for the prediction is $\sqrt{d_x^2 + d_y^2}$, which is the largest Euclidean distance to any of the four neighbouring electrodes from any point within the grid.

Subplot a of Fig 10 are the box plots for the Euclidean distance between predicted and expected peaks for the synthetic moving Gaussian testing data set with different reduction schemes. The proposed euclidean distance error limit for each reduction scheme is shown as the blue line, note how **none** of the 600 total samples along the 6 paths exceed this limit in all x-y dimension peak reduction scheme. Subplot b of Fig 10 shows that the RMSE increases as the number of examples found in the training set decreases.

Individual neural networks were trained using the 25 different σ reduction sets. Subplot a of Fig 11 shows the mean and standard deviations for the Euclidean distance between predicted and expected Gaussian peak locations as a function

of the σ in the training set for the 25 different neural networks. The σ for the moving Gaussian in the testing set is 0.1768 (shown as red star). Note that the in both subplots of Fig 10 prediction results become better as the σ for the reduced training set approaches 0.1768.

D. G3D Decomposition of Recorded HSPs

The 3D matrix of size 9-by-12-by-649 for the left ventricular recording was fitted using 100 G3D components. G3D reconstruction of the recording was done by summing the 100 components. Figure 12 shows fitted G3D isosurfaces for the recording, with further examples in the Supplementary Materials. Over the 649 HSP recording samples, the reconstructed signal from 100 G3D components deviates no more than 5% from the normalized recording when comparing the potential surfaces (9-by-12 x-y axis surface), with a mean of $1.34 \pm 1.30\%$. The isosurfaces of the first 3 fitted G3D components are shown in the bottom row of Figure 12. Note how the 3 components are a part of the summation process to from the final 100 component G3D representation.

E. Prediction of Recorded HSPs

Subplot a of Figure 13 summarizes the RMSE per 2D abstraction slice (x - y plane) between the neural network HSP prediction and expected G3D HSP fit. Here, we expect the G3D fitted HSPs to be the ideal outcome from the neural net, as the testing input to the neural net is the BSPs generated by the forward model from the G3D components of the left ventricular HSP recording. The mean RMSE is $18.5 \pm 5.25\%$. Subplot b from Figure 13 contrasts the predicted HSP time series with its corresponding G3D fit, and normalized actual recording. Figure 14 compares the activation times derived from predicted HSPs and recorded HSPs. The mean absolute difference in activation times across all electrodes was $10.3 \pm 10.8\text{ms}$. The RMSE in predicted activation times is 17.0% .

IV. DISCUSSION

In this paper, we present a proof of concept for a basis function based neural network approach for solving the inverse problem of electrocardiography. We have shown that a neural network can be used to modeling the data relationships between electrical signals on the body and heart surfaces, for a simplified torso model. We trained the neural network with static Gaussian basis and used the neural network to predict synthetic signals and recorded heart surface signals. In the context of our problem the method is robust to noise and perturbed heart locations. This is an important first step for developing a new approach to the inverse problem of electrocardiography.

We have shown that a G3D basis model can effective capture the morphological behavior found within HSPs expressed as a 3D matrix (x , y , t). The G3D basis model offers description of the HSP 3D matrix which improves with the number of G3D components fit (Supplementary Materials), this is a common behavior for basis function models [22]. Due to the smooth

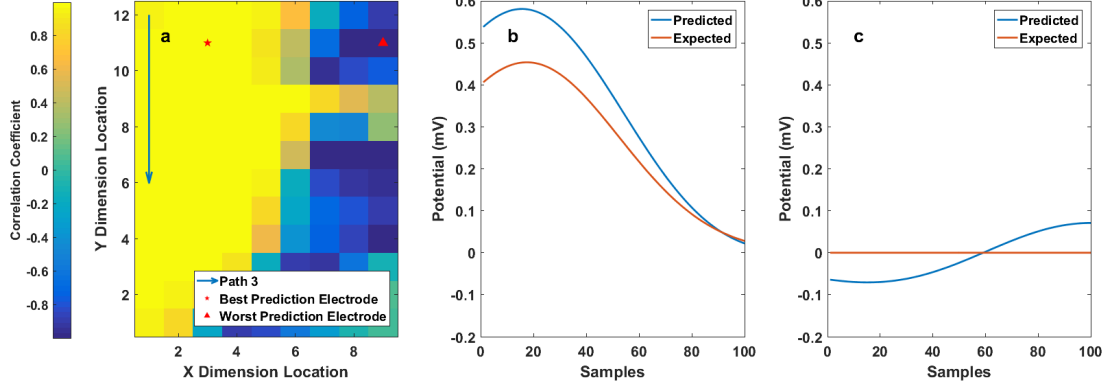


Fig. 5: a) Path 3 on the heart surface 9-by-12 grid, along with the time series correlation between predicted and synthetic data at each electrode. The electrode with the worst prediction in correlation is marked with a red triangle, while the electrode with best prediction in correlation is marked with a red star. b) Time series prediction results for best prediction correlation at electrode ($x = 3, y = 11$) for path 3 in Table II. c) Time series prediction results for worst prediction correlation at electrode ($x = 11, y = 11$) for path 3 in Table II.

nature of the Gaussian basis, its representation of a given recording is fair but not exact, as seen in Figure 12. This is similar to the behavior noted in [16], where small components electrocardiographic signals were sometimes not captured by the Gaussian model. The G3D basis function decomposition technique proposed here is not signal dependent, and can theoretically decompose, and therefore express, HSPs from varying heart states in the same basis function space.

The G3D basis function impulses on the heart surface along with calculated (through the forward model) simultaneous recordings on the body surface allowed for training of a neural network which was able to predict both synthesized HSPs and real-world decomposed HSPs from BSPs. The network performs well when predicting the synthesized moving Gaussian data set described by Table II, with low mean RMSE value of 8.46% across all 6 paths. As the neural net was only trained with basis functions having peaks at integer x and y dimension locations, the prediction error and Euclidean distance is expected to fluctuate in Fig 4 along all 6 paths which include peaks at non-integer x and y dimensions. Interestingly, subplot a of Fig 5 suggests that the time series at electrode locations that are closer to the points of activation (i.e. along the path) achieve better prediction results when compared to electrodes which are far from the point of activation. This is most likely due to the distant electrodes having a close to zero time series (subplot c of Fig 5), which is difficult to predict for an neural net largely trained on impulse or non zero time series data.

The trained neural network is susceptible to noise in the input BSPs as seen in Fig 6. Note that there is a large drop in predicted HSP quality when going from BSP inputs with 20dB to 10dB signal-to-noise ratio in subplot a of Fig 6. Furthermore, subplot b of Fig 6 suggests that, as expected, noisier BSPs will produce noisier HSPs as neural network outputs. However, this is expected as network is trained purely on G3D basis function data without noise. Methods to improve robustness of predictions at signal-to-noise ratios smaller than 20dB will be explored in the future. In subplot a of Fig 7, it shows that the neural network prediction results become increasingly erroneous when predicting testing set HSPs from

hearts that are increasingly distant from the spatial location of the heart used to generate the training set. Encouragingly, the predicted time series in subplot b of Fig 7 show that the shape of the predicted HSP signal is largely unchanged between 0mm and 40mm heart location shifts. Furthermore, in both Fig 7 and Fig 8, there is a non-random change in predicted signal amplitude, peak time, and width as the heart shifts and rotates. Therefore, in the future, there is a possibility of training a generic neural network for solving the cardiac inverse problem for different heart and body geometries by incorporating the geometry information as an input.

Here, we also observe several important factors for constructing an effective training set for prediction of Gaussian basis HSPs using neural nets. We evaluated the effectiveness of training sets based their effect on the Euclidean distance between predicted and expected Gaussian peaks. This is an important measure, as most interesting heart behaviors occur when the electrical potential on the heart surface is non-zero. We show that the maximum Euclidean distance error between predicted and expected Gaussian peaks on the heart surface is related to the distance between Gaussian peaks found in the training set. Specifically, if the training set has examples of peaks at distance d_x in the x dimension of the heart surface, and d_y in the y dimension of the heart surface, then the maximum error in Euclidean distance of the predicted peak is $\sqrt{d_x^2 + d_y^2}$. This limit is made for the proposed model under the assumption that the training set HSP-BSP pairs at neighbouring electrodes are sufficiently different, and the difference between training set HSP-BSP pairs between neighbours' neighbours are larger than for neighbours alone. In Fig 11 we show that the neural network trained on the full training set outperforms any of the neural nets trained on reduced sets with G3D basis functions having a single σ . Therefore, for our proposed data driven model, an effective training set must include a fair representation of data from varying σ values. This is similar to the guidelines for effective training sets proposed by [21].

The neural network prediction of G3D decomposed HSP left ventricular recordings is especially encouraging, as the

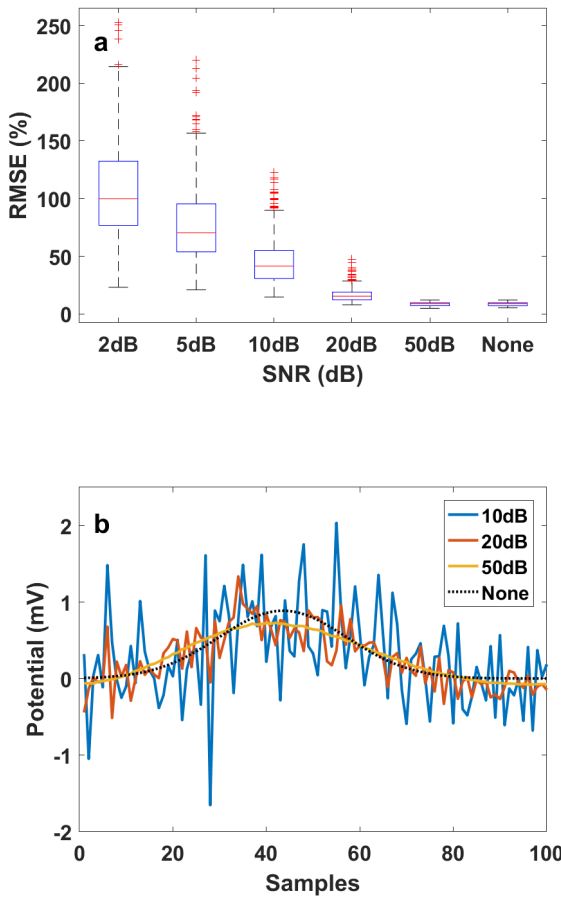


Fig. 6: a) Boxplot of root mean squared (RMSE) value across 2D HSP slices (x - y plane) between predicted and expected HSPs at different noise levels for the input BSP. b) Time series example of predicted HSPs at different BSP noise levels for path 1 from Table II. The expected prediction is the G3D generated moving HSP (blue dotted line).

neural network is trained on the G3D basis function HSPs and forward model BSPs solutions, and **not** via a data set of simultaneously recorded BSPs and HSPs. While the RMSE seen in subplot a of Fig 13 is larger than that found in predictions of synthesized moving G3D HSPs in Fig 4, they are similar to those found for HSPs predicted by other neural networks trained on real-world HSP and BSP data [11], [12]. The dynamic behavior of the recorded HSP is predicted well. This can be seen in the volatile activation within the first 200 samples, the relatively flat period between 200 and 400 samples, and the repolarization period after 400 samples in which the potential returns to baseline for both the recorded and predicted time series in subplot b of Fig 13. This is further supported by the mean absolute difference in predicted and expected activation time being 10.7ms.

Here, we present the prediction of real-world signals based on neural networks trained with basis function data to serve as a case study for how such an approach can be used to solve clinical problems. Our model can be replaced by measurements. When the developing the method a model

reduces some uncertainties. Based on the viability of the data driven method shown here, it is potentially feasible to bypass the forward model for calculating BSPs and train the neural network based on recordings of real world basis function HSPs and their corresponding BSPs in a heart-in-tank experiment in the future. Here, we find that the quality of predictions will increase as the number of HSP-BSP samples pairs in the training set increases. In particular, we show that there is a maximum error in Euclidean distance of predicted Gaussian peaks. This limit can be used to calculate the appropriate distance between stimulus electrodes for real-world HSP-BSP training set recordings to train the proposed model to produce HSP predictions at a desired error level. Furthermore, based on results from the decomposition of HSPs, it seems feasible that BSPs from clinical recordings can be decomposed via fitting techniques into basis functions. These decomposed BSP components can be useful for prediction of clinical HSPs.

V. CONCLUSION

In this work we propose a Gaussian basis function decomposition approach to bypass the rich training data problem of neural network approaches for the inverse problem of electrocardiography. We have shown that a network trained on purely generated basis function HSPs and their respective generated BSPs can be used to predict real world recordings of HSPs decomposed into the same basis function set. Activation maps of the HSPs, predicted from BSPs with a neural network, can be used to identify cardiac dysfunctions during clinical assessments. In future works, this method would be tested on real world HSP Gaussian recordings and their respective BSPs when the data becomes available.

REFERENCES

- [1] B. J. Messinger-Rapport and Y. Rudy, "Regularization of the inverse problem in electrocardiography: A model study," *Math. Biosci.*, vol. 89, no. 1, pp. 79–118, 1988.
- [2] N. Zemzemi and R. Dubois, "A machine learning regularization of the inverse problem in electrocardiography imaging," *Comput. Cardiol. Conf.*, pp. 1135–1138, 2013.
- [3] A. J. Pullan *et al.*, "The Inverse Problem of Electrocardiography," *Compr. Electrocardiol.*, pp. 299–344, 2010.
- [4] S. Ghosh and Y. Rudy, "Application of L1-Norm Regularization to Epicardial Potential Solution of the Inverse Electrocardiography Problem," *Annu. Biomed. Eng.*, vol. 37, no. 5, pp. 902–912, 2009.
- [5] R. Yoram and J. E. Burnes, "Noninvasive electrocardiographic imaging," *Annu. Noninvasive Electrocardiol.*, vol. 4, no. 3, pp. 340–359, 1999.
- [6] A. Malik *et al.*, "A machine learning approach to reconstruction of heart surface potentials from body surface potentials," in *2018 40th Annu. Int. Conf. IEEE Eng. Med. Biol. Soc.*, 2018.
- [7] P. Colli-Franzone *et al.*, "Finite Element Approximation of Regularized Solutions of the Inverse Potential Problem of Electrocardiography and Applications to Experimental Data," *Calcolo*, vol. 22, no. 1, pp. 91–186, 1985.
- [8] ———, "A mathematical procedure for solving the inverse potential problem of electrocardiography. analysis of the time-space accuracy from in vitro experimental data," *Math. Biosci.*, vol. 77, no. 1-2, pp. 353–396, 1985.
- [9] N. Zemzemi *et al.*, "From body surface potential to activation maps on the atria: A machine learning technique," *Comput. Cardiol. (2010)*, vol. 39, pp. 125–128, 2012.
- [10] T. Y. Kwok and D. Y. Yeung, "Constructive algorithms for structure learning in feedforward neural networks for regression problems," *IEEE Trans. Neural Networks*, vol. 8, no. 3, pp. 630–645, 1997.
- [11] K. Bujnarowski *et al.*, "CT-Scan Free Neural Network-Based Reconstruction of Heart Surface Potentials from ECG Recordings," pp. 1–4, 2020.

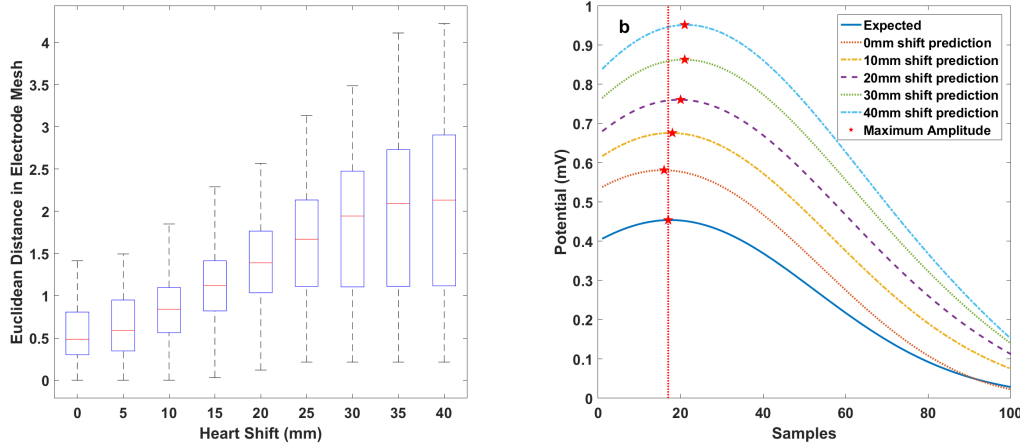


Fig. 7: a) Boxplot of Euclidean distance between predicted and expected peaks of HSPs at different spatial shifts for the heart geometry in the forward model. b) Time series example of predicted HSPs at different shifts in heart geometry for path 3 from Table II. The peaks of the expected outcome from the testing set and the predictions are labelled as red stars. The peak of the expected outcome is also marked as the red dotted vertical line for comparison.

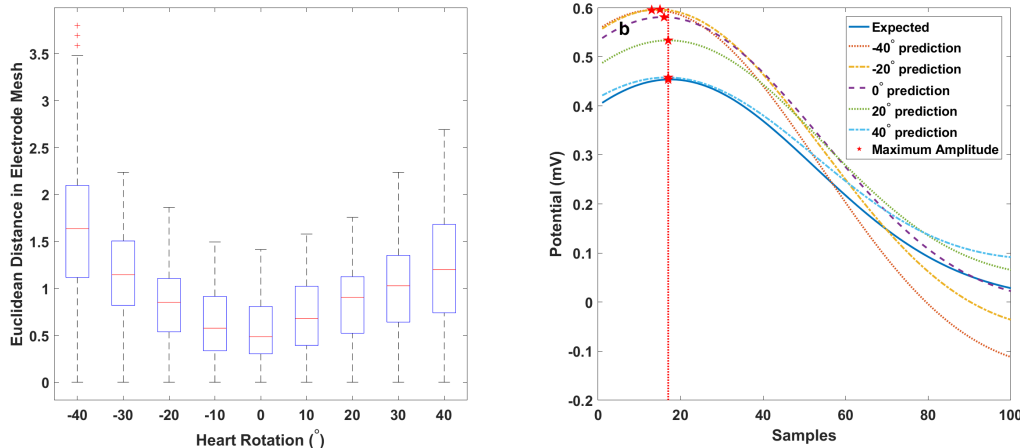


Fig. 8: a) Boxplot of Euclidean distance between predicted and expected peaks of HSPs at different rotation angles for the heart geometry in the forward model. b) Time series example of predicted HSPs at different shifts in heart geometry for path 3 from Table II. The peaks of the expected outcome from the testing set and the predictions are labelled as red stars. The peak of the expected outcome is also marked as the red dotted vertical line for comparison.

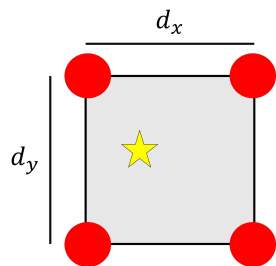


Fig. 9: A small section of the HSP electrode grid, showing 4 neighbouring electrodes. Training set for the neural net contains HSP-BSP pairs with HSPs having Gaussian basis function peaks at the electrodes (shown as red circles). The expected peak of the predicted HSP is somewhere within the grid of four electrodes (shown as a yellow star). The distance between electrodes in the x direction is d_x and the distance between electrodes in the y direction is d_y .

[12] A. Karoui *et al.*, “A Spatial Adaptation of the Time Delay Neural Network for Solving ECGI Inverse Problem,” *Lect. Notes Comput. Sci. (including Subser. Lect. Notes Artif. Intell. Lect. Notes Bioinformatics)*, vol. 11504 LNCS, pp. 94–102, 2019.

- [13] P. E. McSharry *et al.*, “A dynamical model for generating synthetic electrocardiogram signals,” *IEEE Trans. Biomed. Eng.*, vol. 50, no. 3, pp. 289–294, 2003.
- [14] F. Badilini *et al.*, “Automatic analysis of cardiac repolarization morphology using Gaussian mesa function modeling,” *J. Electrocardiol.*, vol. 41, no. 6, pp. 588–594, 2008.
- [15] T. Peng *et al.*, “Parametric Modeling of Electrocardiograms using Particle Swarm Optimization,” in *2018 40th Annu. Int. Conf. IEEE Eng. Med. Biol. Soc.*, 2018, pp. 2695–2698.
- [16] ———, “Predictive modeling of drug effects on electrocardiograms,” *Comput. Biol. Med.*, vol. 108, pp. 332–344, 2019.
- [17] L. R. Bear *et al.*, “Cardiac electrical dyssynchrony is accurately detected by noninvasive electrocardiographic imaging,” *Hear. Rhythm*, vol. 15, no. 7, pp. 1058–1069, 2018.
- [18] G. Cybenko, “Approximation by Superpositions of a Sigmoidal Function,” *Mathematics of Control, Signals, and Systems*, vol. 2, pp. 303–314, 1989.
- [19] K. I. Funahashi, “On the approximate realization of continuous mappings by neural networks,” *Neural Networks*, vol. 2, no. 3, pp. 183–192, 1989.
- [20] L. R. Bear *et al.*, “Forward Problem of Electrocardiography: Is It Solved?” *Circulation: Arrhythmia and Electrophysiology*, vol. 8, no. 3, pp. 677–684, 2015.
- [21] R. Thirumalainambi and J. Bardina, “Training data requirement for a neural network to predict aerodynamic coefficients,” *Indep. Compon. Anal. Wavelets, Neural Networks*, vol. 5102, p. 92, 2003.

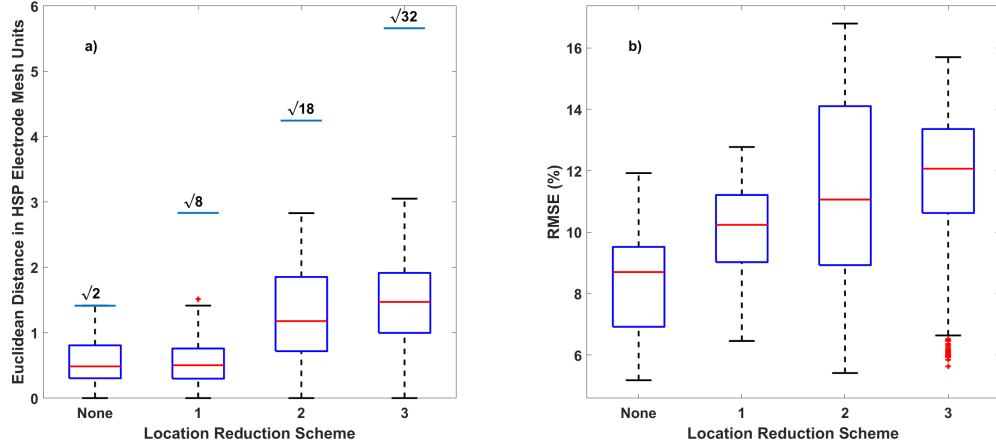


Fig. 10: Box plot representation of prediction error using neural networks trained with training sets reduced with schemes as shown in Fig 3. The left-most box plot with no training data reduction scheme corresponds to error found from all 6 paths found using the full training set. a) Euclidean distance in the x - y plane between predicted and expected Gaussian peak locations for the synthetic moving Gaussian testing data set. The proposed limits on maximum Euclidean distance between predicted and expected Gaussian peaks is shown as the blue line for each box plot. b) RMSE per 2D slice.

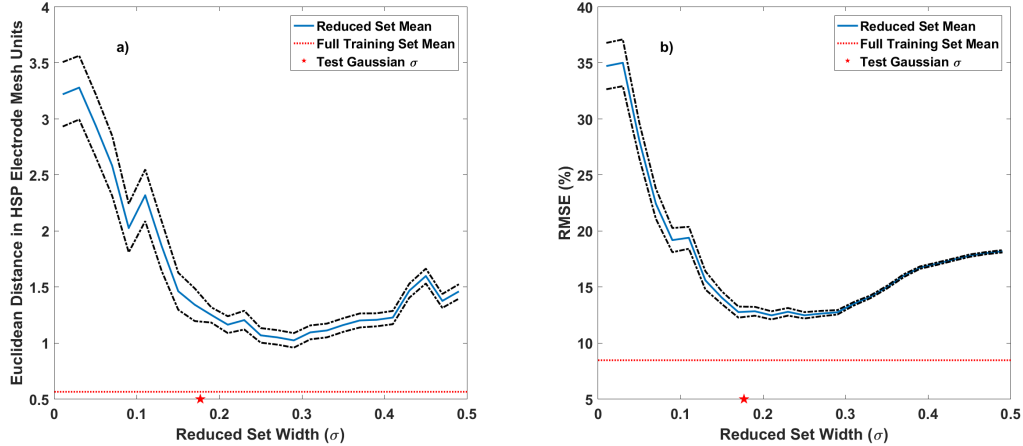


Fig. 11: The mean of the errors when predicted using neural networks trained with σ reduction scheme sets is shown as the blue solid line, the 95% confidence intervals are marked by the black dotted lines. The σ of the testing set Gaussian is shown as the red star. For comparison, the mean of the errors when the full training set is used is the red dotted line. a) Euclidean distance in the x - y plane between predicted and expected Gaussian peak locations for the synthetic moving Gaussian testing data set; b) RMSE per 2D slice.

- [22] E. K. Roonizi and R. Sameni, "Morphological modeling of cardiac signals based on signal decomposition," *Comput. Biol. Med.*, vol. 43, no. 10, pp. 1453–1461, 2013.
- [23] L. S. Lee *et al.*, "Department of Electrical and Computer Engineering Part IV Research Project Project Report Project Number : 10 Deep Learning Neural Nets for Detecting Heart Activity," Tech. Rep., 2018.

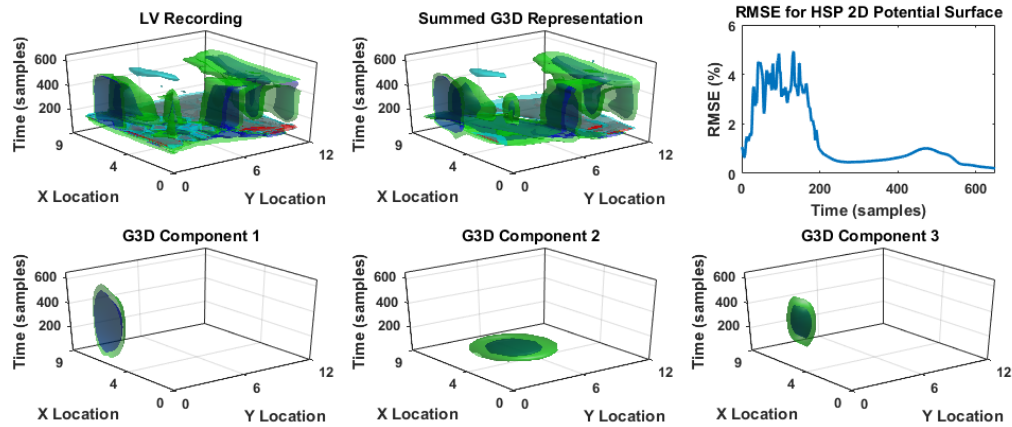


Fig. 12: Top row from left to right shows the isosurface for the full 9-by-12-by-649 matrix for the left ventricular recording, the isosurface of the full G3D representation using 100 components, and the RMSE per 2D slice (x - y plane) for the fitted signal. Bottom row shows the isosurfaces for the first 3 G3D components fitted. The isosurfaces are drawn at values of -0.1, -0.05, 0.05, and 0.1 to show the various potentials found within the 3d signal matrices.

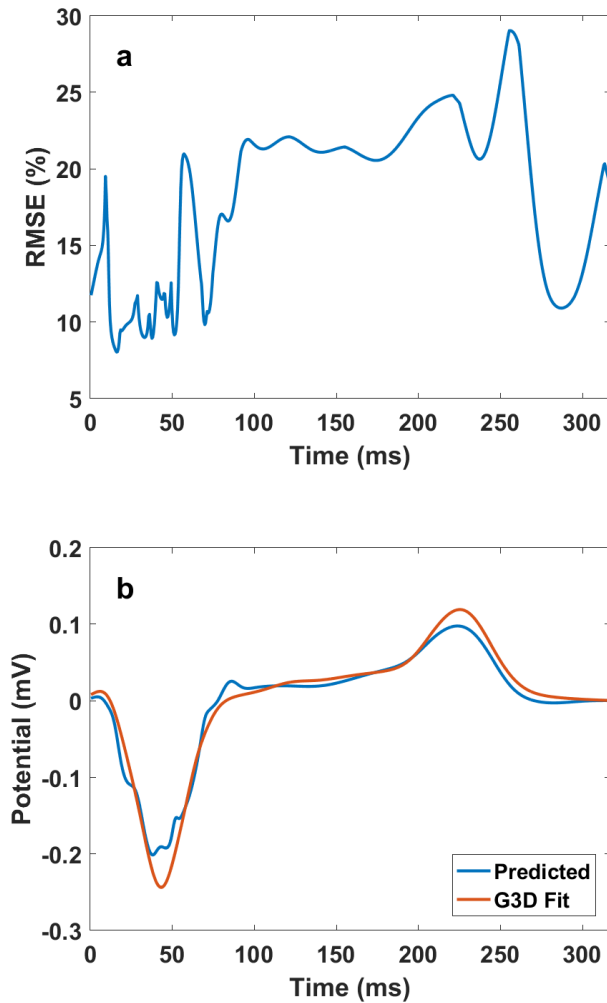


Fig. 13: a) RMSE values per HSP 2D slice between the neural network predicted and expected G3D fit potentials for each temporal sample of the left ventricular averaged beat recording. b) Time series examples of predicted HSPs for the left ventricular average beat recording at electrode ($x = 7$, $y = 11$). The G3D fit HSP is the ideal prediction from the neural network (trained based on G3D basis functions only). The normalized recorded HSP is also presented as a reference.

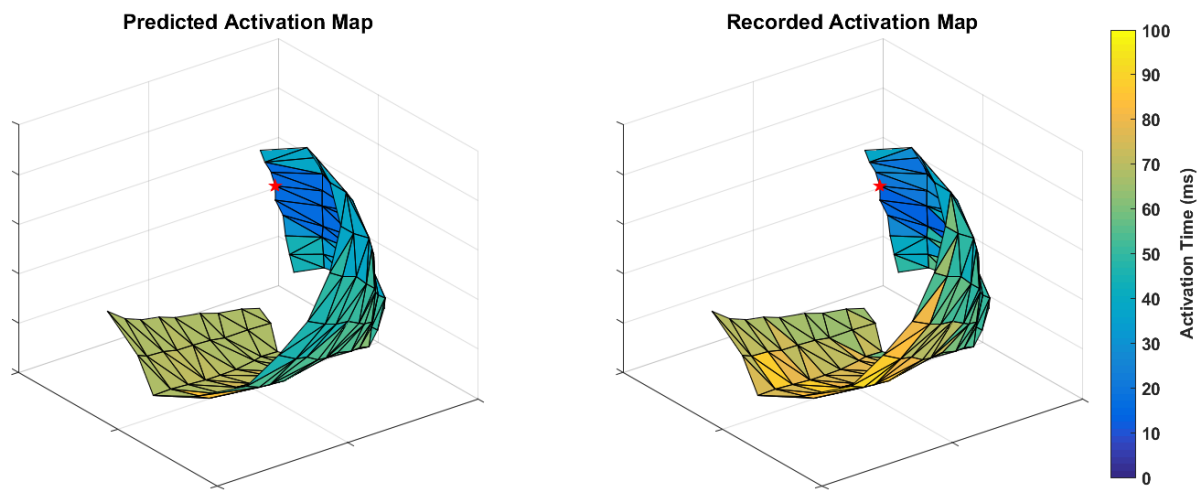


Fig. 14: 3D activation map mesh comparison of the activation maps produced from predicted HSP (Left) and real world recording (Right). The electrode closest to the point of activation (left ventricle) is marked as the red star.

Supplementary Materials

A. Overall Methodology

An overview of the methodology is shown in Figure S1.

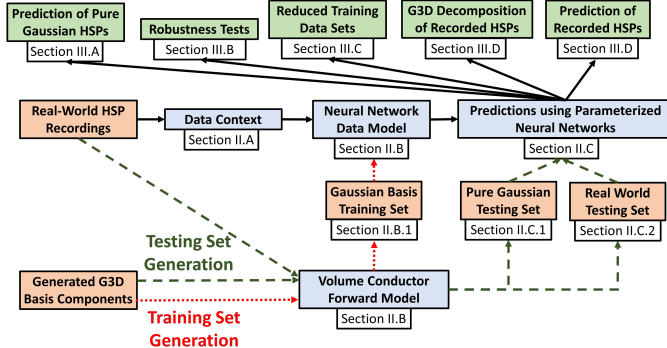


Fig. S1: Summary of methodology.

B. Body and Heart Surface 2D Projections

We performed 2D geometry projections for the heart surface electrodes and body surface electrodes separately for each instance in time. At every instance in time, there are 108 HSP and 128 BSP electrode potential values. The heart surface electrodes were projected onto an evenly spaced 9-by-12 mesh as shown in Fig S2. Using this heart 2D projection, the LV paced averaged beat HSP was projected into a 3D array of size 9-by-12-by-649. The body mesh from the experimental data was used to project the body surface electrodes onto a cylinder approximation of the body using *PointCloud* in MATLAB [23], as shown in Fig S3. The cylinder was unwrapped via a cut along the left anterior descending artery line identified in the experimental data. Bad leads identified via the experimental data were removed. The 2D unwrapped cylinder surface was re-sampled onto a 16-by-16 mesh via linear interpolation using *griddata* in MATLAB.

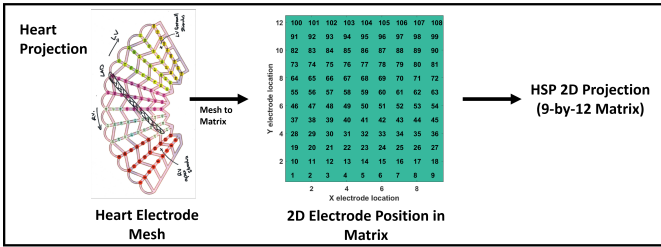


Fig. S2: Summary of heart electrode 2D projection, where electrodes in a mesh were projected into 9-by-12 matrix positions.

C. G3D Library

A combination of different G3D parameters were used to create a G3D library which can describe a wide range of signal shapes and sizes. Here, the G3D basis functions within the library all have an *Amp* of 1. The μ_x was allowed to vary in 8 even locations between 1 and 9 (9 is the size of the x dimension for signal to be fitted). The μ_y was allowed to vary

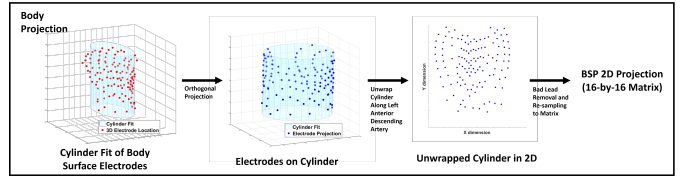


Fig. S3: Summary of body electrode 2D projection. Electrodes in 3D space were first projected onto a cylinder. The cylinder was then unwrapped along the left anterior descending artery line. The unwrapped 2D surface was then re-sampled into 16-by-16 matrix positions.

in 8 even locations between 1 and 12 (12 is the size of the y dimension for signal to be fitted). The μ_t was allowed to vary evenly in 2, 4, 8, 16, 32, 64 splits between 0 and 1 (t has units in heart beat time, varies between 0 and 1). The σ_{xy} was allowed to vary evenly in 2, 4, 8, 16, 32, 64 splits between 0 and 0.5. The σ_t was allowed to vary evenly in 2, 4, 8, 16, 32, 64 splits between 0 and 1. The final G3D library contained G3D basis functions generated from all given combinations of the 6 parameters.

D. Synthetic Moving G3D Paths

Figure S5 summarizes the synthetic moving Gaussian paths along with their respective contours at 3 points in time for each of the 6 paths found in Table II. The 2D representation of these paths on the 9-by-12 heart projection surface can be seen in Fig S4.

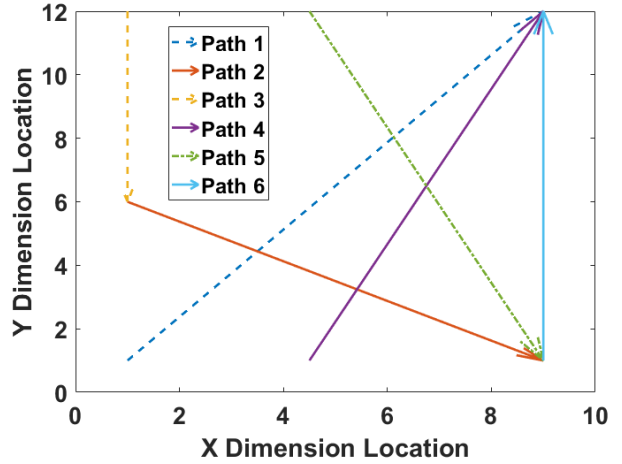


Fig. S4: Synthesized moving Gaussian data paths on the HSP surface (9-by-12). The synthesized data have Gaussians with peaks along these indicated paths, smoothly translating from the start point to end point in 100 samples.

E. G3D Decomposition Representation

Fig S6 shows that error of the summed basis function representation of the HSP signal decreases as the number of G3D's components fit to the signal increase. This is expected as each new basis function was only fit to the unexplained part of the signal in an iterative process.

Fig S7 shows the fitted G3D component isosurfaces for the 9-by-12-by-649 HSP matrix. In the subplots, the number of

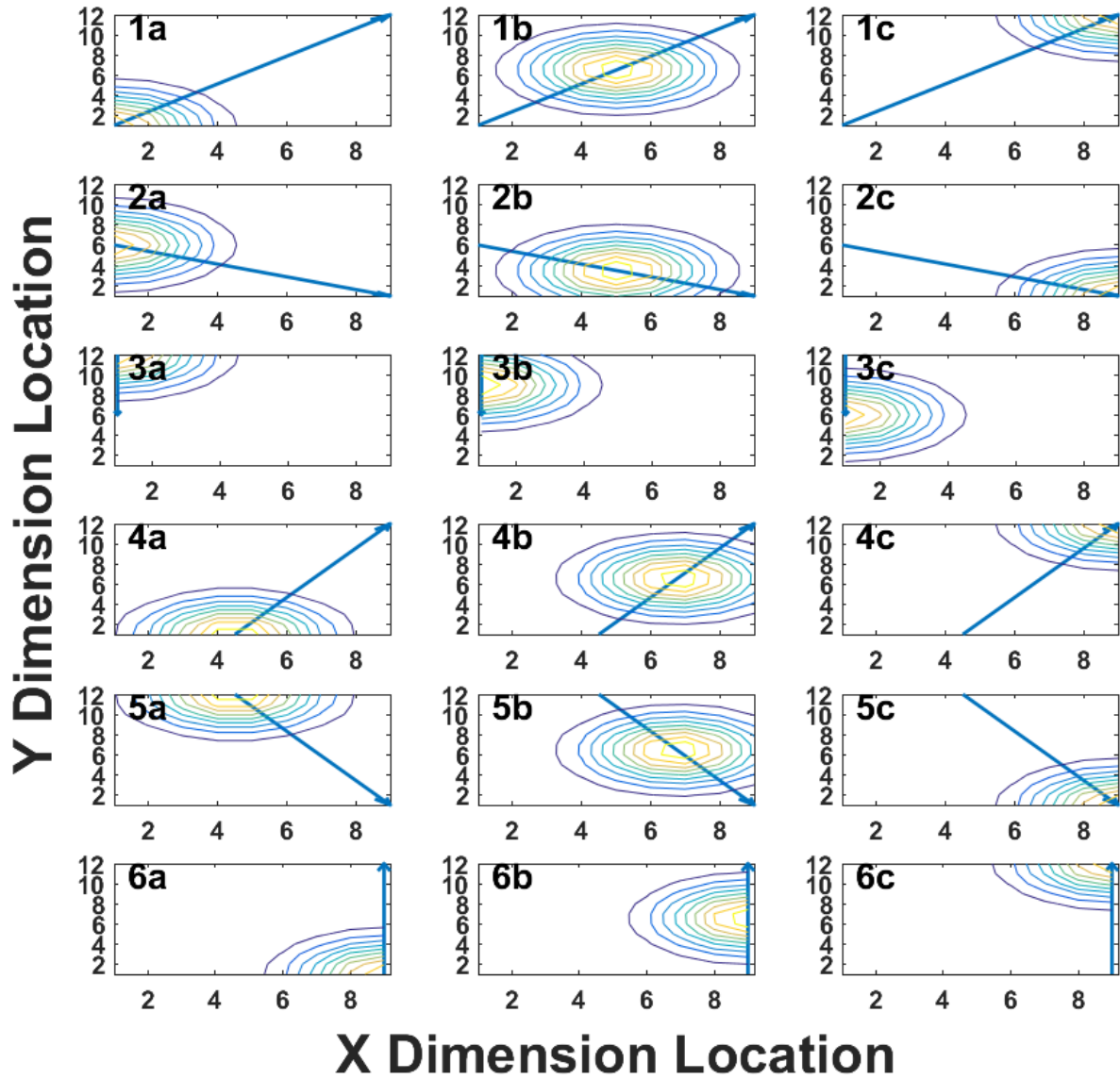


Fig. S5: Synthetic moving Gaussian paths (100 samples in total length each) along with contours at 3 points in time. The subplot labels are the path number followed by a) 1st sample, b) 50 samples in, c) last sample.

summed components progressively increase. Note how the iso-surface begins to resemble that from the actual recording from Figure 12 as the number of summed components increase, which indicates better representation of the original recording.

Subplot a from Fig S8 shows the similarities in morphology and scale between G3D reconstructed and recorded HSP time series for the electrode at $x=7$, $y=11$. Subplot b from Fig S8 presents a subset of 5 G3D waves at electrode $x=7$, $y=11$ which were used to reconstruct the G3D fit time series shown in subplot a.

F. Neural Network Training and Validation Loss

Fig S9 shows the mean squared error loss for both the training and validation sets over the 100 epochs.

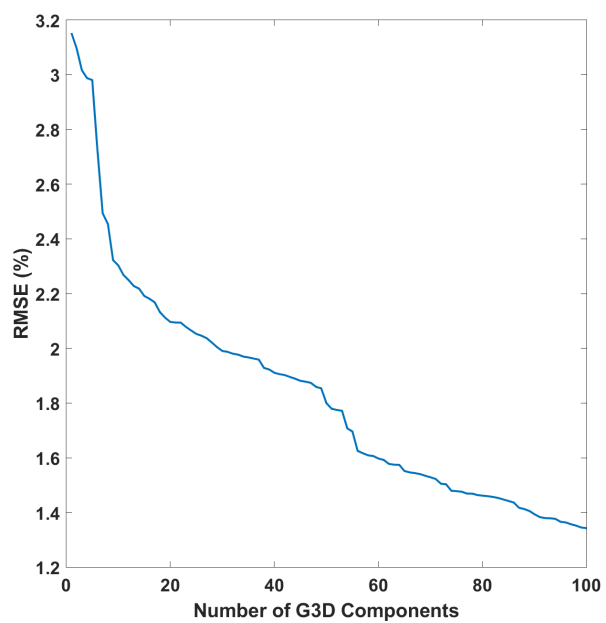


Fig. S6: RMSE of whole left ventricular average beat recording 3D Array per G3D components fit.

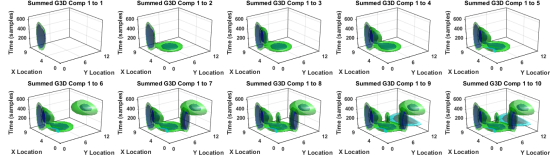


Fig. S7: Summed isosurface of the first 10 G3D components. Each subplot presents the partial sum of the G3D representation of the HSP matrix with the given components in the title.

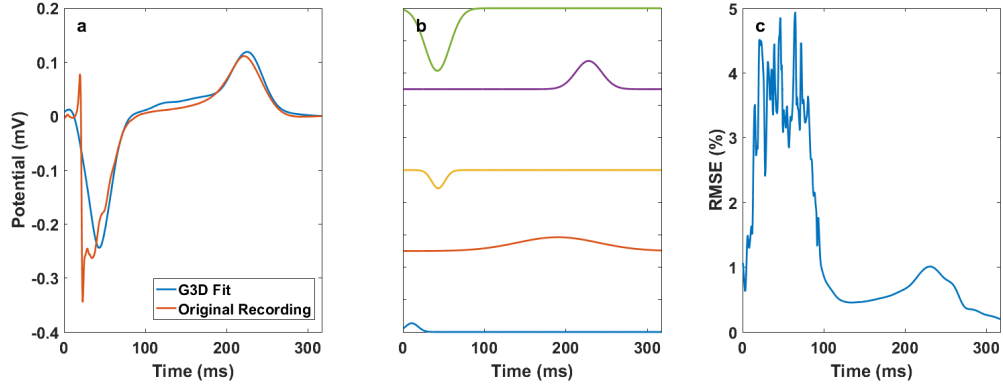


Fig. S8: a) Time series comparison between G3D fit and left ventricular averaged beat HSP at electrode position $x = 7, y = 11$ b) Five largest fitted G3D components in amplitude at electrode $x = 7, y = 11$ as time series. c) RMSE for 2D sample slices (along x-y axis) for the 100 G3D component fit of left ventricular averaged beat HSP.

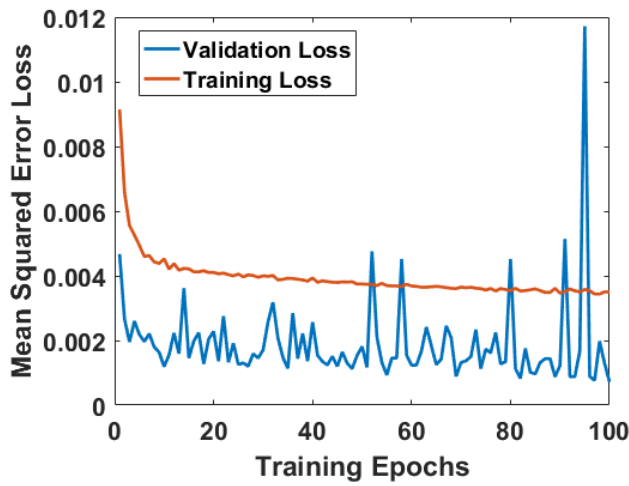


Fig. S9: Mean squared error loss for both the training and validation sets over the 100 training epochs.